

SPECKLE INTERFEROMETRY AT SOAR IN 2019

ANDREI TOKOVININ

Cerro Tololo Inter-American Observatory,* Casilla 603, La Serena, Chile

BRIAN D. MASON

U.S. Naval Observatory, 3450 Massachusetts Ave., Washington, DC, USA

RENE A. MENDEZ

Universidad de Chile, Casilla 36-D, Santiago, Chile

EDGARDO COSTA

Universidad de Chile, Casilla 36-D, Santiago, Chile

ELLIOTT P. HORCH[†]

Department of Physics, Southern Connecticut State University, 501 Crescent Street, New Haven, CT 06515, USA

Draft version May 13, 2020

ABSTRACT

The results of speckle interferometric observations at the 4.1 m Southern Astrophysical Research Telescope (SOAR) in 2019 are given, totaling 2555 measurements of 1972 resolved pairs with separations from 15 mas (median 0^{''}.21) and magnitude difference up to 6 mag, and non-resolutions of 684 targets. We resolved for the first time 90 new pairs or subsystems in known binaries. This work continues our long-term speckle program. Its main goal is to monitor orbital motion of close binaries, including members of high-order hierarchies and *Hipparcos* pairs in the solar neighborhood. We give a list of 127 orbits computed using our latest measurements. Their quality varies from excellent (25 orbits of grades 1 and 2) to provisional (47 orbits of grades 4 and 5).

Keywords: binaries:visual

1. INTRODUCTION

We report here a large set of double-star measurements made at the 4.1 m Southern Astrophysical Research Telescope (SOAR) with the speckle camera, HRCam. This paper continues the series published by Tokovinin, Mason, & Hartkopf (2010a, hereafter TMH10), Tokovinin et al. (2010b), Hartkopf et al. (2012), Tokovinin (2012), Tokovinin et al. (2014), Tokovinin et al. (2015), Tokovinin et al. (2016a), Tokovinin et al. (2018), and Tokovinin et al. (2019). The aims are outlined in these papers and briefly recalled below. The data were taken during 2019. They are presented in the same format as in Tokovinin et al. (2019).

Section 2 reviews all speckle programs executed at SOAR in 2019. The results are presented in Section 3 in the form of electronic tables archived by the journal. We also discuss new resolutions and provide a large list of new orbital elements. A short summary in Section 4 closes the paper.

2. OBSERVATIONS

2.1. Observing programs

As in previous years, HRCam (see Sect. 2.2) was used during 2019 to execute several observing programs, some with common (overlapping) targets. Table 1 gives an overview of these programs and indicates which observations are published in the present paper. Here is a brief description of these programs.

Orbits of resolved binaries are of fundamental importance in various areas of astronomy, e.g. for direct measurement of stellar masses, binary statistics, astrometry, and objects of special interest such as binaries hosting exo-planets. Observations of tight pairs with fast motion, mostly nearby dwarfs, are prioritized at SOAR. However, classical visual binaries are also observed at low cadence to improve their orbits. The Sixth Catalog of Visual Binary Star Orbits, VB6 (Hartkopf, Mason & Worley 2001), contains a substantial fraction of poorly determined, low-grade orbits based on inaccurate and/or sparse visual micrometric measures. This situation is slowly improving. Our work has added many orbits to VB6, more are given here in Section 3.3.

Hierarchical systems of stars challenge the theories of binary-star formation. Better observational data on their statistics and architecture (orbits, relative inclinations) are needed (Tokovinin 2018b). Many hierarchies have been discovered at SOAR using HRCam, and we are following their orbital motion. This paper adds several newly discovered hierarchies and several orbits of subsys-

*National Science Foundation's National Optical-Infrared Astronomy Research Laboratory

Electronic address: atokovinin@ctio.noao.edu

Electronic address: brian.d.mason@navy.mil

Electronic address: rmendez@u.uchile.cl

[†]Adjunct Astronomer, Lowell Observatory

Electronic address: horche2@southernct.edu

Table 1
Observing programs executed with HRCam in 2019

| Program | PI | <i>N</i> | Publ. ^a |
|----------------------------|---------------------|----------|--------------------|
| Orbits | Mason, Tokovinin | 996 | Yes |
| Hierarchical systems | Tokovinin | 188 | Yes |
| Hipparcos binaries | Mendez, Horch | 737 | Yes |
| Neglected binaries | R. Gould, Tokovinin | 363 | Yes |
| Binaries in Upper Scorpius | Tokovinin, Briceño, | 485 | Pub |
| Nearby K,M dwarfs | E. Vrijmoet | 453 | No |
| TESS follow-up | C. Ziegler | 785 | Pub |
| Young moving groups | A. Mann | 645 | No |
| Stars with RV trends | B. Pantoja | 48 | No |

^a This column indicates whether the results are published here (Yes), previously (Pub), or deferred to future papers (No).

tems.

Hipparcos binaries (Perryman et al. 1997) within 200 pc are monitored with the aim of determining orbits and masses for stars in a wide range of effective temperatures and metallicities, as outlined by Horch et al. (2015, 2017, 2019). The southern part of this sample is addressed at SOAR (Mendez et al. 2017). This program overlaps with the general work on orbits.

Accurate parallaxes of visual binaries combined with good-quality orbits will allow accurate measurements of stellar masses. However, the parallactic and orbital motions are coupled. The second *Gaia* data release, DR2 (Gaia collaboration 2018), uses only a linear 5-parameter astrometric model and contains examples of biased parallaxes and proper motions of tight visual binaries. Including acceleration and higher-order terms in the astrometric solution will improve the situation, but the ultimate astrometric precision will be reached only when the orbit is explicitly included in the astrometric model. Considering the limited duration of the *Gaia* mission, ground-based coverage is and will remain essential for accurate measurements of stellar masses.

Neglected binaries with small separations from the Washington Double Star Catalog, WDS (Mason et al. 2001) are observed with a low priority, as a “filler”. Lists of pairs in need of fresh data are provided by R. Gould. A fraction of these stars are interesting because they are presently very tight, near the periastron of their orbits. Some of these pairs contain additional, previously unknown, components.

Members of the Upper Scorpius association were surveyed in a systematic way by Tokovinin & Briceño (2020) to find multiplicity fraction and the distribution of periods and mass ratios, taking advantage of the high productivity of HRCam. The work started in 2018. A total of 614 targets were observed during 2018 and 2019 using approximately two nights of telescope time. Several interesting results are reported in the above paper. Moreover, new close pre-main sequence pairs with fast orbital motion are excellent candidates for measuring masses and testing evolutionary models of young stars.

Nearby K and M dwarfs were observed for E. Vrijmoet. His program aims at determination of a large number of orbits to throw new light on the statistics of orbital elements. As these stars are nearby, some have very short orbital periods and displayed a substantial orbital motion during 2019.

TESS follow-up was one of the major observing programs during 2019. Its first results are published by

Ziegler et al. (2020), but observations continued since the submission of this paper, and the number of surveyed TESS objects of interests has almost doubled.

If observations of a given star were requested by several programs, they are published here even if the other program still continues. We also publish measurements of previously known pairs resolved during surveys, for example in the TESS follow-up.

2.2. Instrument and observing procedure

The observations reported here were obtained with the *high-resolution camera* (HRCam) – a fast imager designed to work at the 4.1 m SOAR telescope (Tokovinin 2018a). The camera was mounted on the SOAR Adaptive Module (SAM, Tokovinin et al. 2016b). The laser guide star of SAM was not used, the deformable mirror of SAM was passively flattened, and the images are seeing-limited. **However, the atmospheric dispersion corrector (ADC) inside SAM was critical for getting good-quality data.** In most observing runs, the median image size was $\sim 0''.6$. The transmission curves of HRCam filters are given in the instrument manual.¹ We used mostly the near-infrared *I* filter (824/170 nm) and the Strömgren *y* filter (543/22 nm); two measures were made in the *R* filter (596/121 nm) **and two in the H α filter (657.3/5 nm).**

For each observing run, a selection of suitable targets from all programs was made. It contains accurate coordinates and proper motions (PMs) to allow for precise pointing of the telescope. The slews are commanded from the custom observing tool that helps to maximize the observing efficiency. When the slew angle is small, the next object is acquired almost immediately. Most observations were taken in the narrow $3''$ field with the 200×200 region of interest (ROI), without binning, in the *I* filter; the *y* filter was used mostly for brighter and/or closer pairs. The pixel scale is $0''.01575$ and the exposure time is normally 24 ms (it is limited by the camera readout speed). Pairs wider than $\sim 1''.4$ are observed in a 400×400 ROI, and the widest pairs are sometimes recorded with the full field of 1024 pixels ($16''$) and 2×2 binning. However, the speckle contrast drops very strongly at separations above $3''$, substantially reducing the quality of measures of wide pairs. Binning is used mostly for the fainter targets; it does not result in the loss of resolution in the *I* band, which ranges from 40 to 45 mas, depending on the magnitude and conditions. Bright stars can be resolved and measured below the formal diffraction limit by fitting a model to the power spectrum and using observations of point sources as reference. The resolution and contrast limits of HRCam are further discussed in TMH10 and in previous papers of this series. For each target, two data cubes of 400 frames are normally recorded and processed independently. This ensures reliability of results despite occasional problems like cosmic ray spikes or telescope vibration.

The first observations reported here were obtained in 2019 January, and the last in 2019 December, in 9 observing runs. HRCam was used during scheduled observing time, but also in parts of engineering nights available from other work. The total number of observations in 2019 (including reference stars) is 5964; the vast major-

¹ <http://www.ctio.noao.edu/soar/sites/default/files/SAM/\discretion>

ity (5242) are made in the I filter, while for bright and close pairs we used the y filter (714 observations). The full set of the 2019 data counts 3199 measurements of 2774 resolved pairs, mostly (but not entirely) published here. Almost all targets are brighter than $I = 12$ mag, although several fainter pairs were measured under very good seeing.

2.3. Data processing and calibration

The data processing is described in TMH10 and Tokovinin (2018a) and briefly recalled here. We use the standard speckle interferometry technique based on the calculation of the power spectrum and the speckle auto-correlation function (ACF) derived from it. Companions are detected as secondary peaks in the ACF and/or as fringes in the power spectrum. Parameters of the binary and triple stars (separation ρ , position angle θ , and magnitude difference Δm) are determined by modeling the observed power spectrum. Additionally, the true quadrant is found from the shift-and-add images, whenever possible.

The pixel scale and angular offset are determined by observations of several relatively wide calibration binaries. Their motion is modeled based on previous observations at SOAR, with individual scale and orientation corrections for each observing run. The models are adjusted iteratively (the latest adjustment in 2019 November). Measurements of wide calibrators by *Gaia* show very small systematic errors (Tokovinin et al. 2019). Typical rms deviations of observations of calibrators from their models are 0.2° in angle and 1 to 3 mas in separation. The position accuracy strongly depends on the target characteristics (larger errors at large Δm and for faint pairs), as well as on the seeing and telescope vibration.

Figure 1 plots the magnitude difference vs. separation for pairs resolved in the I filter (a similar plot was given in Tokovinin et al. 2019). The upper envelope gives a clear idea of the typical contrast limit vs. separation. Several points above the envelope correspond to very difficult tight pairs with a large ΔI ; these measures, made at or beyond the limit of the technique, have large errors. Note points to the left of the formal diffraction limit (vertical dotted line, 41 mas).

3. RESULTS

3.1. Data tables

The results (measures of resolved pairs and non-resolutions) are presented in the same format as in Tokovinin et al. (2019). The long tables are published electronically; here we describe their content.

Table 2 lists 2555 measures of 1972 resolved pairs and subsystems, including the new discoveries. The pairs are identified by their WDS codes and discoverer designations adopted in the WDS catalog (Mason et al. 2001), as well as by alternative names in column (3), mostly from the *Hipparcos* catalog. Equatorial coordinates for the epoch J2000 in degrees are given in columns (4) and (5) to facilitate matching with other catalogs and databases. In the case of resolved multiple systems, the position measurements and their errors (columns 9–12) and magnitude differences (column 13) refer to the individual pairings between components, not to their photo-centers. As in the previous papers of this series, we list the internal errors derived from the power spectrum model and

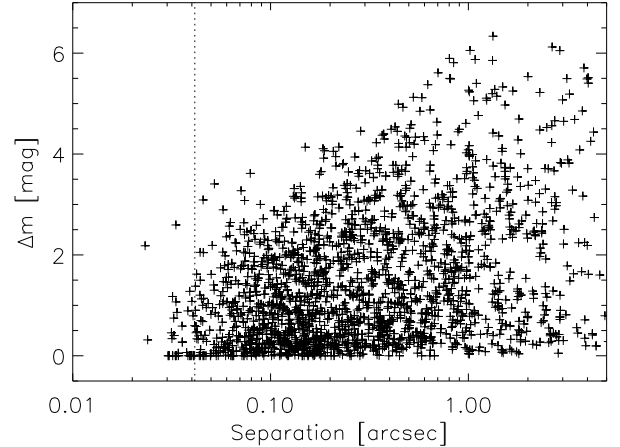


Figure 1. Magnitude difference in the I band vs. separation for pairs resolved in this filter. The vertical dotted line marks the formal diffraction limit of 41 mas.

Table 2
Measurements of double stars at SOAR

| Col. | Label | Format | Description, units |
|------|---------------------|--------|---|
| 1 | WDS | A10 | WDS code (J2000) |
| 2 | Discov. | A16 | Discoverer code |
| 3 | Other | A12 | Alternative name |
| 4 | RA | F8.4 | R.A. J2000 (deg) |
| 5 | Dec | F8.4 | Declination J2000 (deg) |
| 6 | Epoch | F9.4 | Julian year (yr) |
| 7 | Filt. | A2 | Filter |
| 8 | N | I2 | Number of averaged cubes |
| 9 | θ | F8.1 | Position angle (deg) |
| 10 | $\rho\sigma_\theta$ | F5.1 | Tangential error (mas) |
| 11 | ρ | F8.4 | Separation (arcsec) |
| 12 | σ_ρ | F5.1 | Radial error (mas) |
| 13 | Δm | F7.1 | Magnitude difference (mag) |
| 14 | Flag | A1 | Flag of magnitude difference ^a |
| 15 | $(O-C)_\theta$ | F8.1 | Residual in angle (deg) |
| 16 | $(O-C)_\rho$ | F8.3 | Residual in separation (arcsec) |
| 17 | Ref. | A8 | Orbit reference ^b |

^a Flags: q – the quadrant is determined; * – Δm and quadrant from average image; : – noisy data.

^b References to VB6 are provided at <http://ad.usno.navy.mil/wds/orb6/wdsref.txt>

from the difference between the measures obtained from two data cubes. The median error is 0.4 mas, and 90% of errors are less than 1.8 mas. The real errors are usually larger, especially for difficult pairs with substantial Δm and/or with small separations. Residuals from orbits (Section 3.3) and from the models of calibrators, typically between 1 and 5 mas rms, characterize the external errors of the HRcam astrometry.

The flags in column (14) indicate cases when the true quadrant is determined (otherwise the position angle is measured modulo 180°), when the photometry of wide pairs is derived from the long-exposure images (this reduces the bias caused by speckle anisoplanatism) and when the data are noisy or the resolutions are tentative (see TMH10). For binary stars with known orbits, the residuals to the latest orbit and its reference are provided in columns (15)–(17). This work is referenced as SOAR2019.

Non-resolutions are reported in Table 3. Its first columns (1) to (8) have the same meaning and format as in Table 2. Column (9) gives the minimum resolvable

Table 3
Unresolved stars

| Col. | Label | Format | Description, units |
|------|------------------|--------|-----------------------------------|
| 1 | WDS | A10 | WDS code (J2000) |
| 2 | Discov. | A16 | Discoverer code |
| 3 | Other | A12 | Alternative name |
| 4 | RA | F8.4 | R.A. J2000 (deg) |
| 5 | Dec | F8.4 | Declination J2000 (deg) |
| 6 | Epoch | F9.4 | Julian year (yr) |
| 7 | Filt. | A2 | Filter |
| 8 | N | I2 | Number of averaged cubes |
| 9 | ρ_{\min} | F7.3 | Angular resolution (arcsec) |
| 10 | $\Delta m(0.15)$ | F7.2 | Max. Δm at $0''.15$ (mag) |
| 11 | $\Delta m(1)$ | F7.2 | Max. Δm at $1''$ (mag) |
| 12 | Flag | A1 | : marks noisy data |

separation when pairs with $\Delta m < 1$ mag are detectable. It is computed from the maximum spatial frequency of the useful signal in the power spectrum and is normally close to the formal diffraction limit λ/D . The following columns (10) and (11) provide the indicative dynamic range, i.e. the maximum magnitude difference at separations of $0''.15$ and $1''$, respectively. The last column (12) marks noisy data by the flag “.”.

Table 2 contains 90 pairs resolved for the first time; some of those were confirmed in subsequent observing runs. Additional first resolutions belonging to the projects led by other PIs will be reported elsewhere (these pairs are not published here), while new pairs discovered in Upper Scorpius are published by Tokovinin & Briceño (2020). In the following sub-section we discuss the new pairs.

3.2. New pairs

Table 4
New double stars

| WDS | Name | ρ (arcsec) | Δm (mag) | Program ^a |
|------------|-----------------|--------------------|---------------------|----------------------|
| 00160–4816 | HIP 1276 | 0.19 | 0.4 | HIP |
| 00271–3634 | HIP 2136 | 0.18 | 0.5 | HIP |
| 00406–4831 | HIP 3186 | 0.04 | 0.8 | HIP |
| 00457–6752 | HIP 3579 | 0.08 | 2.6 | HIP |
| 01043–5741 | SUB 1 Aa,Ab | 0.22 | 0.7 | HIP |
| 01180–4809 | HIP 6075 | 0.32 | 1.5 | HIP |
| 01376–0223 | RST4181 BC | 0.15 | 0.0 | WDS |
| 02050–3748 | HIP 9713 | 0.34 | 3.1 | HIP |
| 02065+0002 | HIP 9827 | 0.05 | 2.3 | REF |
| 02143–4952 | HIP 10421 | 0.08 | 0.0 | HIP ^b |
| 02442–5234 | HIP 12775 | 1.33 | 4.4 | REF |
| 02466–3232 | HIP 12954 | 1.33 | 3.8 | HIP |
| 02595–6415 | HIP 13935 | 0.51 | 4.6 | HIP |
| 03274–4113 | HIP 16097 | 0.17 | 2.6 | HIP |
| 03405+0508 | STF 430 Aa,Ab | 0.20 | 3.0 | REF |
| 03476–3625 | KPP2826 Aa,Ab | 0.45 | 3.2 | HIP |
| 03566–3313 | HIP 18457 | 0.09 | 0.2 | HIP |
| 04157–5631 | UC 1144 Aa,Ab | 0.19 | 2.3 | HIP |
| 04249–3445 | DAM1313 Aa1,Aa2 | 0.06 | 1.8 | REF |
| 05222–3218 | HIP 25085 | 0.07 | 2.6 | HIP |
| 06203–3004 | 1 CMa | 0.04 | 0.0 | SB |
| 06225–6342 | HIP 30310 | 0.33 | 0.1 | HIP |
| 06237–3319 | HIP 30410 | 0.07 | 0.1 | HIP ^b |
| 06357–7006 | HJ 3885 Aa,Ab | 0.13 | 2.0 | WDS |
| 06404–8223 | HIP 31931 | 1.66 | 2.5 | HIP |
| 06460–6624 | HIP 32414 AB | 0.31 | 3.1 | HIP |
| 06460–6624 | HIP 32414 BC | 0.13 | 0.2 | HIP ^b |
| 07165–5513 | HIP 35203 | 0.17 | 1.6 | HIP ^b |
| 07343–4517 | HIP 36818 | 0.09 | 3.0 | HIP |
| 07480–1924 | B 1077 Ba,Bb | 0.12 | 0.7 | WDS |

Table 4 — *Continued*

| WDS | Name | ρ (arcsec) | Δm (mag) | Program ^a |
|------------|-----------------|--------------------|---------------------|----------------------|
| 07548–6613 | HIP 38645 | 0.06 | 0.0 | HIP ^b |
| 08032–5401 | HIP 39391 | 0.96 | 2.7 | HIP ^b |
| 08134–4534 | HIP 40269 | 0.04 | 0.0 | HIP ^b |
| 08170–3525 | HIP 40569 | 0.38 | 4.3 | HIP |
| 08422–6852 | HIP 42709 | 0.67 | 1.8 | HIP |
| 08507–3825 | JSP 308 Aa,Ab | 0.14 | 2.7 | WDS |
| 09012+0157 | CRC 57 Aa,Ab | 0.19 | 1.3 | MSC |
| 09086–2960 | HIP 44868 | 1.68 | 5.3 | HIP |
| 09350–7804 | KOH 85 AC | 1.80 | 4.7 | WDS |
| 09448–3633 | HIP 47808 | 0.30 | 3.4 | HIP |
| 09538–6719 | HIP 48528 | 0.36 | 3.2 | HIP ^b |
| 09589–5000 | HIP 48928 AB | 1.37 | 1.9 | HIP ^b |
| 09589–5000 | HIP 48928 Aa,Ab | 0.06 | 0.0 | HIP ^b |
| 10152–5846 | HU 1596 BC | 0.23 | 2.4 | WDS |
| 10212–1736 | HIP 50701 | 1.08 | 3.4 | HIP |
| 10231–5032 | HIP 50861 | 1.06 | 3.6 | HIP ^b |
| 10343–7807 | HIP 51748 | 3.39 | 7.2 | HIP |
| 10377–1103 | HIP 52023 | 0.44 | 3.6 | HIP ^b |
| 10560–0254 | HIP 53443 | 0.10 | 1.8 | HIP ^b |
| 11177+2722 | HIP 55170 | 0.07 | 1.4 | REF |
| 11415–7703 | HIP 57027 | 0.09 | 0.1 | REF |
| 11428–3549 | HIP 57129 | 1.26 | 2.5 | HIP |
| 11515–2138 | HIP 57827 | 0.11 | 1.2 | HIP ^b |
| 11565–5046 | HIP 58226 | 0.75 | 3.1 | HIP ^b |
| 12114–1647 | S 634 Aa,Ab | 0.023 | 0.7 | SB |
| 12407–4803 | HIP 61868 | 0.06 | 1.7 | HIP ^b |
| 12556–6900 | HDS1813Aa,Ab | 0.05 | 1.6 | HIP |
| 13103–3248 | HIP 64264 | 1.78 | 3.6 | HIP ^b |
| 13240–5253 | HIP 65385 AB | 1.70 | 2.0 | HIP |
| 13240–5253 | HIP 65385 Aa,Ab | 0.29 | 0.3 | HIP |
| 13372–2337 | HIP 66433 | 0.28 | 3.7 | REF |
| 14062–6543 | SKF 107 Aa,Ab | 0.98 | 3.6 | HIP |
| 14079–3736 | HIP 69026 | 0.29 | 4.5 | HIP |
| 14219–3609 | HIP 70214 | 1.09 | 3.9 | HIP |
| 14333–2707 | HDS2056 Ba,Bb | 0.05 | 0.2 | HIP ^b |
| 14333–3054 | HIP 71162 | 0.24 | 3.2 | HIP ^b |
| 14336–0956 | HIP 71188 | 1.28 | 3.3 | HIP |
| 14347–3528 | HIP 71289 | 0.08 | 0.1 | REF |
| 14386–0710 | HIP 71600 | 0.44 | 4.2 | HIP ^b |
| 14397–0957 | HIP 71685 | 1.48 | 4.1 | HIP |
| 15031–4200 | B 1257 BC | 0.15 | 0.8 | MSC |
| 15031–4237 | WIS 279 Aa,Ab | 0.25 | 2.0 | HIP ^b |
| 15107–4344 | CPO 415 Aa,Ab | 1.39 | 5.1 | REF |
| 15594–3020 | HIP 78313 | 0.65 | 2.5 | HIP |
| 16103–2209 | HIP 79244 | 0.03 | 0.6 | REF ^b |
| 16358–5345 | KPP3002 Aa,Ab | 1.17 | 2.6 | HIP ^b |
| 16486–3715 | HIP 82272 | 0.84 | 5.8 | REF |
| 16520–3602 | HIP 82521 AB | 0.39 | 1.5 | HIP |
| 16520–3602 | HIP 82521 Aa,Ab | 0.09 | 0.9 | HIP |
| 17522–2440 | HIP 87453 | 2.65 | 6.1 | HIP |
| 18431+0742 | LDS 1013 BC | 0.39 | 0.9 | MSC |
| 18568–3002 | KPP4129 Aa,Ab | 0.13 | 2.0 | HIP ^b |
| 20363–1856 | TOK 339 Aa,Ab | 1.67 | 2.4 | HIP |
| 20516–2927 | HIP 102963 | 1.49 | 5.3 | HIP ^b |
| 22247–6537 | HIP 110630 | 0.14 | 3.1 | REF ^b |
| 22374–4550 | SKF 384 Aa,Ab | 0.21 | 4.0 | HIP ^b |
| 22419–3155 | HIP 112064 | 0.12 | 0.0 | HIP ^b |
| 23232–5441 | HIP 115455 | 1.62 | 2.6 | HIP ^b |
| 23257–4537 | HIP 115648 | 0.26 | 2.4 | HIP ^b |
| 23308–4724 | HIP 116045 | 0.23 | 2.4 | HIP ^b |

^a HIP – *Hipparcos* suspected binary; MSC – multiple system; REF – reference star; SB – spectroscopic binary; WDS – neglected pair.

^b Confirmed.

Table 4 highlights the 90 first-time resolutions of double stars or new subsystems by listing their approximate separations at discovery time, magnitude differences (mostly in the I band), and the corresponding observing programs. Full measurements of these pairs are found in the Table 2. Most new pairs (66) are *Hippar*-

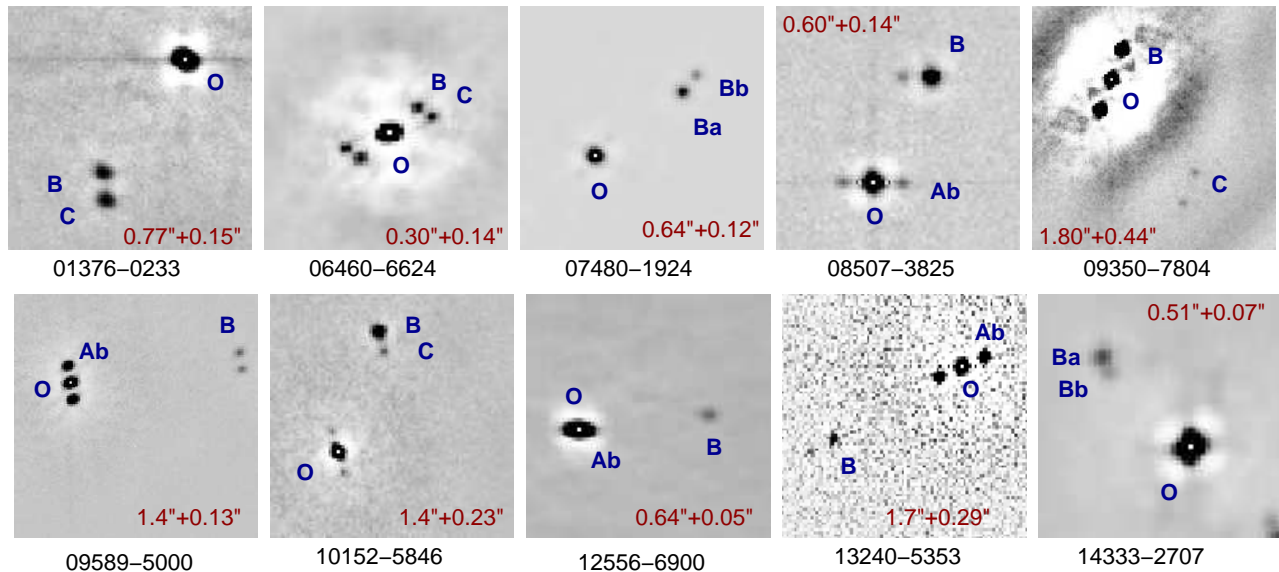


Figure 2. Triple systems discovered in 2019. Fragments of the speckle ACFs in arbitrary negative intensity scale are shown. The peaks corresponding to the components are marked, the central peak (white dot at coordinate origin) is labeled O. Separations of the wide and close pairs in arcseconds indicate the spatial scale.

cos suspected binaries. We also resolved serendipitously 12 reference stars. Seven subsystems in the previously known WDS pairs, also discovered accidentally, have the program code WDS. New resolutions are either very tight pairs or wider pairs with a large contrast; all “easy” pairs with comparable components and large separations were already discovered, e.g. by *Hipparcos*.

As in previous papers of this series, we discovered new visual multiple systems with three or more resolved components. This information will be ingested into the current version of the multiple-star catalog, MSC (Tokovinin 2018b). In the case of HIP 48928 (J09589–5000) and HIP 65385 (J13240–5253), both inner and outer pairs are new discoveries. Figure 2 presents fragments of the speckle ACFs of some multiple systems. Three new wide and faint companions to previously known closer pairs (J03302–7024, J09350–7804, and J09589–5000) are optical, as revealed by *Gaia* DR2 by their discrepant proper motions and/or parallaxes. Similarly, the known 4^h2 pair SKF 107 (J14062–6543) is optical, while the chance of the new 1^h pair being physical is higher.

New tight binaries are promising candidates for orbit determination. HIP 79244 (J16103–2209) shows fast motion during one year. The bright spectroscopic binary HIP 30122 (J06203–3004, 1 CMA) with a period of 675 days was observed on request by J. Docobo and securely resolved into a 35-mas near-equal pair. Its single-lined spectroscopic orbit should be upgraded to a double-lined one to allow measurement of the orbital parallax.

3.3. New and updated orbits

Speckle measurements at SOAR are used to compute new and improve previously known orbits. The well-known difficulties inherent to visual binaries (insufficient coverage, inaccurate or misleading measures) resulted in the large number of poor-quality orbits in the general orbit catalog, VB6 (Hartkopf, Mason & Worley 2001). The situation is improving as new, substantially more accurate data become available. At the same time, many first-time orbits just computed from recent observations

are tentative (grades 4 or 5) and contribute to the pool of poor orbits in the catalog as the older orbits become better known. In some cases, the lack of coverage leaves long-period orbits poorly constrained despite good modern measures. Nevertheless, even tentative (and possibly wrong) orbits are useful in several ways: as a synthesis of all existing data, for predicting binary positions and planning future measurements, etc.

In Table 5, orbital elements and their errors are given for 93 pairs observed in 2019. Formal grades and references to previous orbits are given in the last columns (SOAR2019 for the orbits computed here). Asterisks mark orbits where radial velocities from the literature are used jointly with position measures. The complementary Table 6 lists 34 provisional, poorly constrained orbits of grades 4 and 5 without errors, which in this case are large or even misleading. For circular and/or face-on orbits, some Campbell elements become degenerate and they are fixed accordingly. Some reliable orbits of grades 3 or better resulting from our work were already published in the Information Circulars (e.g. Tokovinin 2019). However, the Circulars do not provide errors of the elements, so we publish these orbits here with errors to give the full result (some with a slight adjustment using the latest measures). Orbit correction is a continuous process. Note that Table 5 also contains 25 orbits of excellent quality (grades 1 and 2). The official grades consider several factors (see Hartkopf, Mason & Worley 2001) and are not uniquely correlated with errors of the elements. For this reason, 16 low-grade orbits with reasonably small errors are kept in Table 5.

The orbital elements and their errors were determined by the weighted least-squares fit using the IDL program ORBIT (Tokovinin 2016b). We adopt weights proportional to σ^{-2} , where the errors σ are assigned according to the measurement technique (e.g. from 2 to 5 mas for speckle interferometry with 4-m class telescopes, 10 mas for *Hipparcos*, 50 mas or larger for visual micrometer measures) and corrected iteratively to reduce the impact of outliers, if necessary. In some cases the pub-

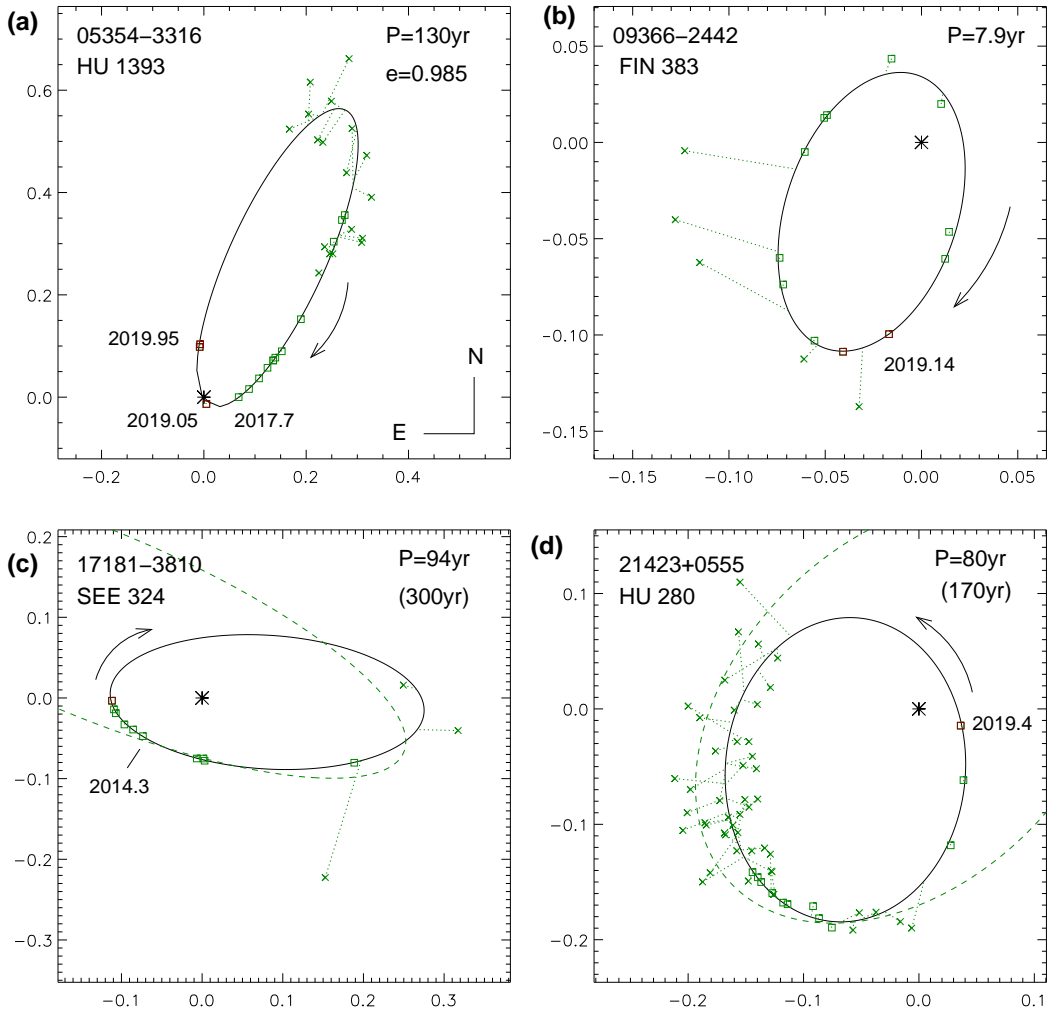


Figure 3. Orbits of “classical” visual binaries observed at SOAR in 2019. In this and following Figures, the axis scale is in arcseconds, the primary component (asterisk) is located at the coordinate origin. Green squares denote accurate speckle-interferometric measures of the secondary component (the 2019 measures are highlighted in red), crosses denote less accurate micrometer measures. The measures are connected to the orbit (ellipse) by short dotted lines. In the two lower panels, the dashed lines are previous orbits.

lished radial velocities (RVs) are used, leading to the combined spectro-interferometric orbits. Mass sums are computed as a sanity check, especially helpful for poorly constrained preliminary orbits. Two pairs (J04303+1950 and J05229-4219) were unresolved in 2019 despite predictions of their previous orbits. These non-resolutions are accounted for by the new, corrected orbits.

Figure 3 gives four noteworthy examples where our observations substantially contributed to the knowledge of orbits of classical visual binaries. Speckle monitoring of J05354-3316 at SOAR (panel a) indicated diminishing separation, and in 2019 the pair passed through the periastron. In 2019.05 it was unresolved; however, the elongated power spectrum was fitted with a fixed $\Delta y = 1.3$ mag, yielding a separation of 15 mas (below the diffraction limit). Two good measures were taken after periastron. The extremely high eccentricity of $e = 0.985 \pm 0.002$ is well constrained by our data. If the periastron had been missed, we would have to wait for 130 years for the next one. The case of J09366-2442 in panel (b) shows how unreliable or even misleading the visual measures of close pairs can be. Including these measures in the orbital fit would spoil the result, while the speckle

data alone define the orbit quite well. The period of J17181-3810 (panel c) was revised from 300 to 94 yr. This pair was not observed at all for 69 years, from 1897 till 1966, which is rather unusual. Based on three micrometer measures and only a few speckle data available in 2014, the previous 300 yr orbit by Tokovinin et al. (2015) was just a bold guess! Now the elements are constrained better, but the long period means that this orbit will remain poorly known for decades. Yet another case of radical orbit revision (from 170 to 80 yr) is J21423+0555 (panel d). This pair now rapidly moves through the periastron and in a few more years its eccentric orbit will become definitive.

To illustrate the impact of SOAR observations on the knowledge of stellar masses, we plot in Figure 4 four well-constrained orbits of nearby M-type dwarfs, continuing the work of Mason et al. (2018). Full analysis of mass-luminosity relation is outside the scope of this paper, and the orbits are highlighted here only to illustrate the potential of HRCam data in this area. The spectral types in the Figure are retrieved from Simbad. All orbits except the last one were known previously, but with a lower accuracy. For example, for J10367+1522

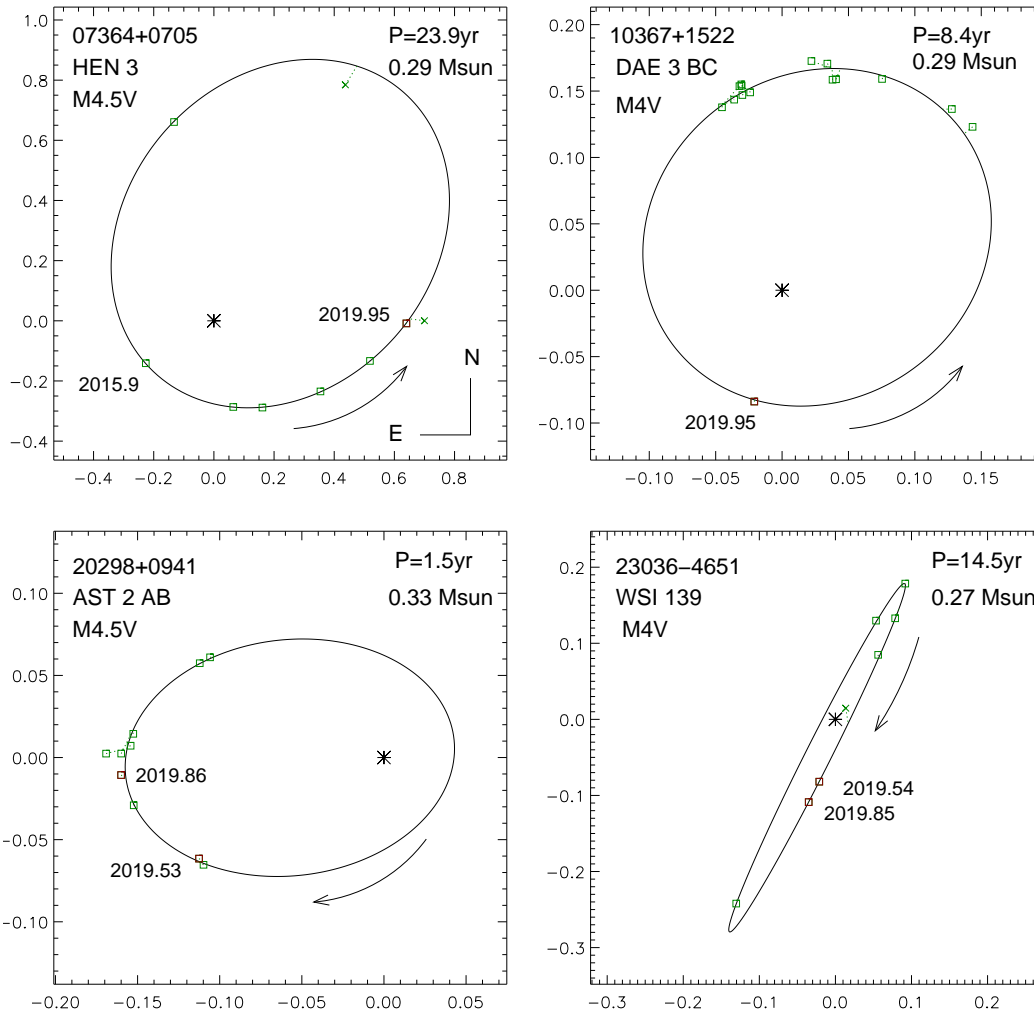


Figure 4. New orbits of four M4V dwarf binaries. The mass sum computed from the orbital elements and parallax is indicated. (DAE 3 BC) Calissendorff et al. (2017) found an excess of mass which is not confirmed by our new orbit, constrained nicely by the 2019 measure. This is a triple system of M dwarfs at 20 pc where the outer orbit is also computed, although it is still poorly constrained. In contrast, J20298+0941 (GJ 791.2), previously listed in the WDS as a tight visual triple AB+AC, is in fact a simple binary, never resolved as triple at SOAR or elsewhere; another companion D at $9''$ is optical. We used the RVs and position measures by Benedict et al. (2016) to get a well-constrained combined orbit. The RVs, however, are likely biased because the resulting orbital parallax of 93 ± 3 mas contradicts the accurate parallax measured by the same authors (113.4 ± 0.2 mas), while the mass ratio of 0.5 inferred from the RV amplitudes contradicts $\Delta J = 2.3$ mag measured at SOAR. The *Gaia* parallax, 133.8 ± 1.4 mas, is obviously biased by the orbit. The last pair of M-dwarfs in Figure 4, J23036-4651 (WSI 139), did not have previous orbit determinations. Nevertheless, its 14.5 yr orbit based almost entirely on the SOAR data is already quite reliable; the rms residuals are 2 mas.

Figure 5 illustrates the emerging combined spectro-interferometric orbit of J05066-7736 (HIP 23776). Astrometric orbit with a period of 1.9 yr based on *Hipparcos* was published by Goldin & Makarov (2006). Our orbit with a period of 2.18 yr and a semimajor axis of 53.1 ± 0.9 mas is strongly constrained by three measures taken in 2019. All measures come from SOAR, and the rms residuals to the orbit are 1.1 mas. High-resolution spectroscopy (to be reported elsewhere) yields RV measurements of both components. The preliminary orbital parallax is 26.4 ± 1.1 mas and the masses are 0.89 and 0.83 solar. The *Gaia* parallax is 28.68 ± 0.18 mas. Continued speckle interferometry and spectroscopy of this pair during another year will lead to accurate mass measurement. The spectral type G8VFe-1.6CH-1.2 suggests chemical peculiarity, while the fast proper motion of $0'.45 \text{ yr}^{-1}$ is typical of halo or thick disk stars. Nordström et al. (2004) measured the metallicity $[\text{Fe}/\text{H}]$ of -0.47 and determined the mass ratio of 0.89 ± 0.01 ; our preliminary orbit gives the mass ratio of 0.93 ± 0.01 .

Table 5
Visual orbits

| WDS <i>HIP</i> | Discov. | P (yr) | T (yr) | e | a (arcsec) | Ω (deg) | ω (deg) | i (deg) | Grade | Ref. ^a |
|-------------------|---------|-------------|-------------|-------|-----------------|-------------------|-------------------|--------------|-------|-------------------|
| 00121-5832 | RST4739 | 36.91 | 1989.95 | 0.597 | 0.236 | 55.0 | 278.2 | 147.4 | 3 | Tok2019h |

Table 5 — *Continued*

| WDS HIP | Discov. | P (yr) | T (yr) | e | a (arcsec) | Ω (deg) | ω (deg) | i (deg) | Grade | Ref. ^a |
|------------|---------------|-------------|-------------|--------------|-----------------|-------------------|-------------------|--------------|-------|-------------------|
| 975 | | ± 0.45 | ± 0.18 | ± 0.026 | ± 0.006 | ± 6.8 | ± 5.7 | ± 3.6 | | |
| 00277–1625 | YR 1 Aa,Ab | 13.35 | 2014.41 | 0.024 | 0.1208 | 167.8 | 270.3 | 69.6 | 4 | Tok2019h |
| 2190 | | ± 0.15 | ± 0.54 | ± 0.019 | ± 0.0020 | ± 0.8 | ± 14.8 | ± 0.9 | | |
| 00462–2214 | RST4155 | 49.27 | 2003.49 | 0.305 | 0.1693 | 177.9 | 141.7 | 138.0 | 2 | Hei1984a |
| 3606 | | ± 1.13 | ± 0.53 | ± 0.022 | ± 0.0044 | ± 4.3 | ± 2.5 | ± 2.3 | | |
| 00550–5315 | RST 23 | 140 | 1973.59 | 0.85 | 0.569 | 182.3 | 79.4 | 105.9 | 4 | SOAR2019 |
| ... | | ± 19 | ± 1.62 | ± 0.09 | ± 0.152 | ± 5.0 | ± 4.5 | ± 5.7 | | |
| 01308–5940 | TOK 183 | 6.586 | 2020.432 | 0.455 | 0.0671 | 352.3 | 42.4 | 93.5 | 3 | Tok2015c |
| 7040 | | ± 0.059 | ± 0.079 | ± 0.017 | ± 0.0013 | ± 0.6 | ± 2.8 | ± 0.8 | | |
| 02038–0020 | TOK 38 Aa,Ab | 5.660 | 2005.426 | 0.367 | 0.0377 | 271.9 | 30.5 | 71.7 | 3 | SOAR2019* |
| 9631 | | ± 0.006 | ± 0.020 | ± 0.006 | ± 0.0009 | ± 2.1 | ± 1.0 | ± 3.8 | | |
| 02290–1959 | RST2280 Aa,Ab | 31.41 | 2020.69 | 0.686 | 0.557 | 185.2 | 38.7 | 154.1 | 3 | Tok2018i |
| 11565 | | ± 0.24 | ± 0.07 | ± 0.014 | ± 0.012 | ± 8.4 | ± 8.8 | ± 3.2 | | |
| 02305–4342 | ELP 1 Aa,Ab | 14.42 | 2020.0 | 0.032 | 0.130 | 122.3 | 14.7 | 139.7 | 3 | Tok2018c |
| ... | | ± 1.36 | ± 5.2 | ± 0.017 | ± 0.008 | ± 5.5 | ± 133.6 | ± 4.1 | | |
| 02517–5234 | HU 1562 | 67.62 | 2019.94 | 0.950 | 0.2588 | 49.1 | 168.9 | 128.9 | 3 | Tok2019h |
| 13341 | | ± 1.07 | ± 0.17 | ± 0.022 | ± 0.0036 | ± 3.5 | ± 6.8 | ± 11.5 | | |
| 03271+1845 | CHR 10 AB | 16.88 | 1994.4 | 0.040 | 0.0787 | 91.2 | 206.7 | 42.8 | 3 | Ole1999 |
| 16077 | | ± 0.10 | ± 3.3 | ± 0.032 | ± 0.0066 | ± 5.6 | ± 66.1 | ± 6.9 | | |
| 03379+0538 | YSC 27 | 16.51 | 2013.025 | 0.222 | 0.1399 | 98.6 | 94.7 | 123.5 | 3 | Cve2017b |
| 16390 | | ± 0.20 | ± 0.066 | ± 0.012 | ± 0.0015 | ± 1.1 | ± 1.7 | ± 0.7 | | |
| 03462–2423 | RST2321 | 96.26 | 2013.99 | 0.832 | 0.2150 | 11.5 | 155.8 | 43.9 | 3 | SOAR2019 |
| 17600 | | ± 2.43 | ± 0.40 | ± 0.027 | ± 0.0034 | ± 9.6 | ± 10.9 | ± 4.6 | | |
| 04008+0505 | A 1937 | 46.08 | 2014.74 | 0.535 | 0.0974 | 31.9 | 0.4 | 40.8 | 2 | Tok2019h |
| 18374 | | ± 1.04 | ± 0.12 | ± 0.008 | ± 0.0014 | ± 3.0 | ± 3.4 | ± 2.0 | | |
| 04063+1952 | BAG 4 | 15.89 | 2012.25 | 0.921 | 0.0959 | 133.6 | 266.4 | 114.0 | 3 | Bag2001 |
| ... | | ± 0.12 | ± 0.39 | ± 0.010 | ± 0.0025 | ± 8.6 | ± 2.7 | fixed | | |
| 04070–1000 | HDS 521 AB | 21.04 | 2017.938 | 0.712 | 0.2302 | 220.4 | 77.4 | 121.5 | 2 | Tok2019h |
| 19206 | | ± 0.04 | ± 0.025 | ± 0.004 | ± 0.0020 | ± 0.4 | ± 0.3 | ± 0.5 | | |
| 04142–4608 | RST2338 | 18.145 | 2002.715 | 0.631 | 0.1941 | 169.1 | 138.9 | 30.6 | 2 | Doc2016i |
| 19758 | | ± 0.054 | ± 0.088 | ± 0.012 | ± 0.0021 | ± 5.8 | ± 6.5 | ± 1.4 | | |
| 04303+1950 | PAT 10 | 11.016 | 1986.577 | 0.754 | 0.1280 | 127.6 | 34.1 | 142.1 | 4 | SOAR2019* |
| 21008 | | ± 0.020 | ± 0.040 | ± 0.007 | ± 0.0019 | ± 2.6 | ± 3.0 | ± 2.0 | | |
| 04318–2407 | RST2347 | 122.9 | 2010.87 | 0.523 | 0.1734 | 163.5 | 339.7 | 129.4 | 3 | Tok2019h |
| 21133 | | ± 8.2 | ± 0.44 | ± 0.025 | ± 0.0065 | ± 4.5 | ± 5.8 | ± 4.6 | | |
| 04389–1207 | HDS 599 | 50.13 | 2004.18 | 0.817 | 0.3174 | 153.9 | 281.2 | 76.5 | 3 | Tok2019h |
| 21644 | | ± 1.45 | ± 0.30 | ± 0.018 | ± 0.0155 | ± 1.0 | ± 1.0 | ± 0.9 | | |
| 04406–0912 | WOR 17 | 215.5 | 1994.0 | 0.813 | 1.919 | 11.7 | 36.7 | 32.3 | 5 | SOAR2019 |
| 21765 | | ± 20.8 | ± 0.35 | ± 0.014 | ± 0.086 | ± 4.6 | ± 5.1 | ± 3.4 | | |
| 04539–2032 | HDS 633 | 11.834 | 2018.197 | 0.913 | 0.1429 | 167.6 | 157.9 | 56.0 | 3 | Tok2019d |
| 22772 | | ± 0.107 | ± 0.072 | ± 0.013 | ± 0.0042 | ± 5.4 | ± 9.1 | ± 3.1 | | |
| 04553–0352 | RST4257 AB | 87.63 | 2011.40 | 0.566 | 0.2497 | 169.8 | 3.1 | 119.5 | 4 | SOAR2019 |
| ... | | ± 2.48 | ± 0.74 | ± 0.023 | ± 0.0142 | ± 2.9 | ± 4.7 | ± 3.2 | | |
| 05066–7734 | TOK 785 | 2.178 | 2020.088 | 0.181 | 0.0531 | 284.5 | 7.0 | 60.6 | 3 | SOAR2019* |
| 23776 | | ± 0.018 | ± 0.034 | ± 0.014 | ± 0.0009 | ± 1.4 | ± 6.5 | ± 2.2 | | |
| 05069–2135 | DON 93 BC | 115.4 | 2002.63 | 0.339 | 1.209 | 89.6 | 257.6 | 150.0 | 4 | SOAR2019 |
| ... | | ± 3.1 | ± 0.45 | ± 0.030 | ± 0.016 | ± 4.7 | ± 5.6 | ± 3.5 | | |
| 05229–4219 | TOK 93 Aa,Ab | 5.99 | 2013.78 | 0.555 | 0.0625 | 238.2 | 93.4 | 64.4 | 3 | Tok2016e |
| 15148 | | ± 0.12 | ± 0.12 | ± 0.036 | ± 0.0031 | ± 2.8 | ± 1.1 | ± 2.5 | | |
| 05245–0224 | MCA 18 Aa,Ab | 9.414 | 2011.046 | 0.361 | 0.0472 | 125.3 | 12.6 | 103.5 | 2 | Tok2015c |
| 25281 | | ± 0.041 | ± 0.250 | ± 0.018 | ± 0.0016 | ± 1.3 | ± 9.3 | ± 1.8 | | |
| 05272+1758 | MCA 19 Aa,Ab | 15.914 | 2014.60 | 0.806 | 0.0757 | 251.9 | 317.1 | 109.4 | 2 | Jte2018 |
| 25499 | | ± 0.073 | ± 0.16 | ± 0.083 | ± 0.0036 | ± 1.7 | ± 5.6 | ± 7.3 | | |
| 05354–3316 | HU 1393 | 130.0 | 2019.04 | 0.985 | 0.6590 | 205.9 | 73.7 | 113.5 | 3 | FRM2014a |
| 26245 | | ± 4.0 | ± 0.030 | ± 0.002 | ± 0.0515 | ± 1.4 | ± 1.5 | ± 1.8 | | |
| 05365+2556 | CHR 203 | 13.56 | 1993.65 | 0.947 | 0.0848 | 135.9 | 50.0 | 160.0 | 3 | SOAR2019 |
| 26322 | | ± 0.126 | ± 0.299 | ± 0.010 | ± 0.0181 | ± 9.4 | fixed | ± 53.7 | | |
| 06035+1941 | MCA 24 | 13.061 | 2006.52 | 0.808 | 0.0555 | 224.4 | 291.5 | 111.8 | 2 | Msn1997a |
| 28691 | | ± 0.031 | ± 0.16 | ± 0.045 | ± 0.0022 | ± 3.3 | ± 9.2 | ± 7.8 | | |
| 06138–2352 | JNN 50 Ba,Bb | 11.75 | 2020.36 | 0.74 | 0.263 | 18.8 | 295.4 | 120.7 | 4 | SOAR2019 |
| 29568 | | ± 1.03 | ± 0.23 | ± 0.12 | ± 0.020 | ± 12.5 | ± 9.5 | ± 2.1 | | |
| 06146–0434 | CHR 164 Aa,Ab | 18.94 | 2017.28 | 0.762 | 0.0491 | 287.4 | 227.1 | 57.8 | 3 | Tok2019d |
| 29629 | | ± 0.64 | ± 0.29 | ± 0.037 | ± 0.0046 | ± 7.0 | ± 12.1 | ± 6.1 | | |
| 06253+0130 | FIN 343 | 76.76 | 2020.49 | 0.360 | 0.1321 | 165.3 | 153.7 | 161.9 | 3 | Tok2019d |
| 30547 | | ± 3.22 | ± 0.45 | ± 0.014 | ± 0.0023 | ± 21.8 | ± 26.9 | ± 4.6 | | |
| 06573–4929 | RST5253 AB | 50.66 | 2006.36 | 0.038 | 0.2170 | 148.8 | 87.5 | 72.2 | 3 | Hrt2012a |
| 33455 | | ± 1.53 | ± 2.03 | ± 0.032 | ± 0.0041 | ± 0.6 | ± 15.2 | ± 0.7 | | |
| 07312+0210 | TOK 393 | 5.71 | 2015.83 | 0.094 | 0.0606 | 27.3 | 168.4 | 144.2 | 3 | Tok2017c |
| 36557 | | ± 0.14 | ± 0.25 | ± 0.030 | ± 0.0026 | ± 7.8 | ± 19.7 | ± 5.5 | | |
| 07364+0705 | HEN3 | 23.93 | 2016.208 | 0.587 | 0.6402 | 85.7 | 57.8 | 14.4 | 4 | Tok2018e |
| ... | | ± 0.40 | ± 0.008 | ± 0.005 | ± 0.0051 | ± 6.2 | ± 6.4 | ± 1.6 | | |
| 07560+2342 | COU 929 | 45.09 | 1997.98 | 0.4746 | 0.2555 | 186.70 | 70.66 | 71.86 | 1 | Hrt2009 |
| 38755 | | ± 0.19 | ± 0.21 | ± 0.0034 | ± 0.0011 | ± 0.23 | ± 0.73 | ± 0.22 | | |
| 08125–4616 | CHR 143 Aa,Ab | 33.08 | 2017.67 | 0.284 | 0.0723 | 172.7 | 253.5 | 69.9 | 3 | Tok2015c |
| 40183 | | ± 0.46 | ± 0.18 | ± 0.015 | ± 0.0010 | ± 1.0 | ± 2.7 | ± 1.1 | | |
| 08158–1027 | RST3578 AB | 29.37 | 2017.413 | 0.470 | 0.2220 | 93.3 | 216.8 | 59.3 | 3 | Tok2019d |

Table 5 — *Continued*

| WDS HIP | Discov. | P (yr) | T (yr) | e | a (arcsec) | Ω (deg) | ω (deg) | i (deg) | Grade | Ref. ^a |
|------------|---------------|-------------|-------------|---------|-----------------|-------------------|-------------------|--------------|-------|-------------------|
| 40465 | | ±0.09 | ±0.076 | ±0.019 | ±0.0043 | ±1.1 | ±2.4 | ±1.7 | | |
| 08230-7102 | HDS1196 | 19.45 | 2021.85 | 0.63 | 0.0652 | 16.3 | 175.7 | 133.6 | 3 | SOAR2019 |
| 41093 | | ±1.72 | ±1.33 | ±0.25 | ±0.0079 | ±18.6 | ±32.2 | ±24.5 | | |
| 08255-4058 | RST3592 | 133.8 | 2009.420 | 0.512 | 0.1442 | 165.0 | 246.2 | 140.4 | 3 | SOAR2019 |
| ... | | ±19.2 | ±0.46 | ±0.050 | ±0.0179 | ±10.8 | ±11.8 | ±11.1 | | |
| 09252-1258 | WSI 73 | 12.715 | 2018.157 | 0.627 | 0.1294 | 93.1 | 42.7 | 85.9 | 4 | Tok2017b |
| 46191 | | ±0.123 | ±0.059 | ±0.009 | ±0.0025 | ±0.5 | ±2.0 | ±0.4 | | |
| 09366-2442 | FIN 383 | 7.883 | 2017.428 | 0.638 | 0.0814 | 176.2 | 223.7 | 130.9 | 2 | Tok2018b |
| 47159 | | ±0.041 | ±0.037 | ±0.011 | ±0.0020 | ±2.9 | ±3.8 | ±2.3 | | |
| 09439-5738 | HDS1404 Aa,Ab | 21.55 | 2019.79 | 0.723 | 0.1345 | 165.2 | 4.2 | 59.0 | 3 | SOAR2019 |
| 47736 | | ±0.835 | ±0.050 | ±0.018 | ±0.0108 | ±3.5 | ±5.6 | ±2.9 | | |
| 09442-2746 | FIN 326 | 18.390 | 2020.924 | 0.506 | 0.1075 | 175.0 | 138.2 | 126.8 | 2 | Doc2013d |
| 47758 | | ±0.086 | ±0.088 | ±0.015 | ±0.0012 | ±1.8 | ±2.6 | ±0.9 | | |
| 09474+1134 | MCA 34 AB | 15.203 | 2003.96 | 0.3129 | 0.11097 | 203.09 | 22.3 | 76.26 | 2 | Jte2018 |
| 48029 | | ±0.019 | ±0.11 | ±0.0065 | ±0.00084 | ±0.50 | ±2.8 | ±0.49 | | |
| 10116+1321 | HU 874 | 17.974 | 2003.819 | 0.928 | 0.1528 | 111.6 | 317.9 | 82.4 | 2 | Hrt1996a |
| 49929 | | ±0.032 | ±0.092 | ±0.006 | ±0.0055 | ±0.6 | ±2.6 | ±0.8 | | |
| 10345-3721 | RST3706 | 62.6 | 2025.8 | 0.292 | 0.1517 | 40.8 | 324.1 | 103.9 | 3 | SOAR2019 |
| 51760 | | ±6.343 | ±1.773 | ±0.092 | ±0.0183 | ±2.1 | ±17.3 | ±2.3 | | |
| 10367+1522 | DAE 3 BC | 8.427 | 2011.326 | 0.358 | 0.1382 | 104.1 | 44.4 | 21.4 | 4 | Jnn2017b |
| ... | | ±0.029 | ±0.041 | ±0.009 | ±0.0030 | ±10.5 | ±10.2 | ±3.8 | | |
| 10373-4814 | SEE 119 | 16.672 | 2019.819 | 0.771 | 0.3999 | 35.7 | 287.0 | 123.3 | 2 | Tok2019d |
| 51986 | | ±0.032 | ±0.005 | ±0.003 | ±0.0021 | ±0.4 | ±0.3 | ±0.3 | | |
| 10397-3755 | HDS1523 | 59.7 | 2018.40 | 0.698 | 1.014 | 8.0 | 55.5 | 132.5 | 3 | SOAR2019 |
| 52190 | | ±1.24 | ±0.002 | ±0.003 | ±0.015 | ±0.6 | ±0.5 | ±0.6 | | |
| 11053-2718 | FIN 47 AB | 7.612 | 2013.749 | 0.370 | 0.1346 | 45.1 | 156.5 | 94.0 | 2 | Jte2018 |
| 54204 | | ±0.007 | ±0.088 | ±0.013 | ±0.0015 | ±0.4 | ±3.9 | ±0.4 | | |
| 11235+0701 | BAG 24 Aa,Ab | 20.810 | 2014.412 | 0.300 | 0.2275 | 150.0 | 222.0 | 160.0 | 3 | SOAR2019 |
| 55605 | | ±0.074 | ±0.209 | ±0.018 | ±0.0016 | ±16.8 | ±18.9 | fixed | | |
| 11446-4925 | RST9004 AB | 35.43 | 2009.866 | 0.409 | 0.3074 | 139.0 | 350.1 | 27.5 | 2 | Wol2014 |
| 57269 | | ±0.13 | ±0.029 | ±0.003 | ±0.0014 | ±1.8 | ±1.9 | ±0.8 | | |
| 12463-6806 | R 207 AB | 188.0 | 1874.2 | 0.79 | 1.16 | 138.6 | 72.5 | 53.3 | 3 | FMR2012g |
| 62322 | | ±16.5 | ±6.5 | ±0.13 | ±0.23 | ±12.1 | ±11.3 | ±9.9 | | |
| 13190-2536 | HDS1866 | 22.72 | 2008.29 | 0.397 | 0.1435 | 18.3 | 225.8 | 137.8 | 3 | SOAR2019 |
| 64970 | | ±0.37 | ±0.16 | ±0.024 | ±0.0032 | ±5.0 | ±5.4 | ±2.6 | | |
| 13317-0219 | HDS1895 | 3.239 | 2013.781 | 0.534 | 0.0968 | 309.2 | 358.8 | 19.6 | 1 | Hrt2012a* |
| 659820 | | ±0.002 | ±0.006 | ±0.006 | ±0.0007 | ±2.7 | ±3.0 | ±2.3 | | |
| 13334+0919 | HDS1902 | 26.15 | 2008.55 | 0.54 | 0.131 | 124.3 | 309.0 | 27.7 | 3 | SOAR2019 |
| 66132 | | ±0.51 | ±0.44 | ±0.01 | ±0.016 | ±34.2 | ±34.5 | ±15.9 | | |
| 13396+1045 | BU 612 AB | 22.532 | 2019.7346 | 0.5422 | 0.19932 | 36.71 | 356.9 | 45.34 | 1 | Msn1999a |
| 66640 | | ±0.020 | ±0.0023 | ±0.0023 | ±0.00050 | ±0.61 | ±1.1 | ±0.37 | | |
| 13520-3137 | BU 343 AB | 254.8 | 1996.36 | 0.646 | 1.0709 | 187.2 | 242.9 | 135.4 | 3 | Tok2014a |
| 67696 | | ±4.8 | ±0.09 | ±0.005 | ±0.0100 | ±0.6 | ±0.9 | ±0.4 | | |
| 13598-0333 | HDS1962 | 9.764 | 2008.366 | 0.405 | 0.0785 | 34.6 | 235.3 | 57.0 | 2 | Tok2018i |
| 68380 | | ±0.078 | ±0.075 | ±0.014 | ±0.0016 | ±1.6 | ±2.3 | ±1.2 | | |
| 14025-2440 | B 263 AB | 205.9 | 2011.84 | 0.533 | 0.597 | 19.8 | 65.5 | 48.8 | 4 | Tok2015c |
| 68587 | | ±17.8 | ±0.64 | ±0.024 | ±0.037 | ±1.6 | ±4.8 | ±1.7 | | |
| 14035+1047 | GJ 538 | 9.876 | 2011.177 | 0.480 | 0.3156 | 74.0 | 183.0 | 96.9 | 3 | SOAR2019* |
| 68682 | | ±0.002 | ±0.005 | ±0.001 | ±0.0006 | ±0.1 | ±0.2 | ±0.2 | | |
| 14382+1402 | TOK 406 | 8.29 | 2016.044 | 0.373 | 0.0998 | 7.3 | 168.3 | 130.5 | 3 | Tok2018e |
| 71572 | | ±0.14 | ±0.028 | ±0.010 | ±0.0013 | ±1.4 | ±2.0 | ±1.0 | | |
| 14581-4852 | WSI 80 | 22.39 | 2020.52 | 0.791 | 0.4015 | 86.6 | 109.2 | 108.4 | 3 | Tok2015c |
| 73241 | | ±2.08 | ±0.19 | ±0.061 | ±0.0108 | ±3.6 | ±1.1 | ±0.5 | | |
| 16059+1041 | HDS2273 Aa,Ab | 33.00 | 1992.977 | 0.426 | 0.3512 | 160.6 | 234.6 | 35.1 | 3 | Tok2019h |
| 78864 | | ±0.13 | ±0.055 | ±0.004 | ±0.0021 | ±1.2 | ±0.9 | ±0.9 | | |
| 16534-2025 | WSI 86 | 14.91 | 2014.96 | 0.502 | 0.2697 | 13.1 | 26.7 | 132.0 | 4 | SOAR2019 |
| 82621 | | ±0.25 | ±0.17 | ±0.013 | ±0.0059 | ±3.0 | ±5.9 | ±2.3 | | |
| 17156-1018 | BU 957 | 91.1 | 2030.2 | 0.570 | 0.287 | 25.0 | 28.8 | 101.1 | 2 | Tok2015c |
| 84423 | | ±2.9 | ±1.8 | ±0.048 | ±0.013 | ±1.2 | ±4.2 | ±1.1 | | |
| 17181-3810 | SEE 324 | 94.2 | 2020.54 | 0.414 | 0.195 | 266.3 | 179.9 | 117.8 | 3 | Tok2015c |
| 84634 | | ±12.3 | ±1.55 | ±0.028 | ±0.007 | ±1.9 | ±14.1 | ±3.0 | | |
| 17240-0921 | RST3972 Aa,Ab | 15.262 | 2006.017 | 0.570 | 0.1465 | 69.2 | 16.8 | 25.5 | 2 | Sod1999 |
| 85141 | | ±0.018 | ±0.038 | ±0.004 | ±0.0012 | ±3.5 | ±3.9 | ±1.8 | | |
| 17415-5348 | HDS 2502 | 20.39 | 2018.044 | 0.594 | 0.1341 | 158.5 | 321.5 | 136.7 | 3 | Tok2017c |
| 86569 | | ±0.34 | ±0.028 | ±0.008 | ±0.0010 | ±1.6 | ±2.1 | ±1.3 | | |
| 17586-1306 | HU 190 | 162.7 | 2011.40 | 0.422 | 0.3700 | 15.4 | 0.0 | 180.0 | 4 | Tok2019h |
| 88010 | | ±12.3 | ±0.66 | ±0.027 | ±0.0142 | ±3.2 | fixed | fixed | | |
| 18480-1009 | HDS2665 | 38.44 | 2023.47 | 0.411 | 0.4796 | 36.4 | 195.7 | 56.4 | 4 | Tok2016e |
| 92250 | | ±1.22 | ±0.30 | ±0.038 | ±0.0058 | ±2.4 | ±5.5 | ±0.7 | | |
| 20048+0109 | TOK 699 | 7.83 | 2018.578 | 0.241 | 0.1579 | 74.1 | 45.1 | 36.3 | 3 | Tok2018i |
| 98878 | | fixed | ±0.037 | ±0.008 | ±0.0030 | ±3.8 | ±3.6 | ±2.0 | | |
| 20210-1447 | BLA 7 Aa,Ab | 3.762 | 2015.642 | 0.452 | 0.0487 | 43.6 | 124.2 | 75.1 | 2 | Tok2015c |
| 100325 | | ±0.000 | ±0.009 | ±0.009 | ±0.0010 | ±1.3 | ±1.0 | ±2.0 | | |
| 20298+0941 | AST 2 AB | 1.4708 | 2019.185 | 0.573 | 0.1118 | 287.7 | 20.4 | 148.5 | 3 | Tok2019h* |
| ... | | ±0.0004 | ±0.009 | ±0.010 | ±0.0015 | ±2.4 | ±3.6 | ±3.0 | | |
| 20462+1554 | WSI 110 Aa,Ab | 4.871 | 2003.255 | 0.254 | 0.0979 | 143.6 | 344.0 | 78.5 | 3 | SOAR2019* |

Table 5 — *Continued*

| WDS <i>HIP</i> | Discov. | P (yr) | T (yr) | e | a (arcsec) | Ω (deg) | ω (deg) | i (deg) | Grade | Ref. ^a |
|-------------------|---------------|-------------|-------------|--------|-----------------|-------------------|-------------------|--------------|-------|-------------------|
| 102490 | | ±0.001 | ±0.018 | ±0.006 | ±0.0015 | ±1.0 | ±1.5 | ±1.5 | | |
| 21088–0426 | HDS3013 Aa,Ab | 25.019 | 2019.391 | 0.557 | 0.3138 | 153.1 | 99.3 | 134.9 | 3 | Tok2018e |
| 104383 | | ±0.026 | ±0.017 | ±0.007 | ±0.0019 | ±1.5 | ±1.1 | ±0.7 | | |
| 21094–7310 | I 379 AB | 5.389 | 2017.555 | 0.690 | 0.1829 | 194.4 | 183.4 | 93.3 | 2 | SOAR2019 |
| 104440 | | ±0.059 | ±0.041 | ±0.022 | ±0.0040 | ±0.5 | ±3.9 | ±1.5 | | |
| 21130–1133 | VOU 24 AB | 128.5 | 2020.03 | 0.321 | 0.264 | 65.3 | 250.0 | 161.9 | 4 | SOAR2019 |
| ... | | ±8.1 | ±1.93 | ±0.012 | ±0.017 | ±10.2 | fixed | ±12.4 | | |
| 21198–2621 | BU 271 AB | 189.1 | 1841.48 | 0.631 | 2.159 | 244.7 | 190.5 | 65.2 | 3 | Tok2019h |
| 105312 | | ±4.5 | ±4.06 | ±0.021 | ±0.013 | ±1.3 | ±3.8 | ±0.4 | | |
| 21395–0003 | BU 1212 AB | 48.68 | 1972.09 | 0.867 | 0.4277 | 141.1 | 293.6 | 55.2 | 2 | Tok2019h |
| 106942 | | ±0.34 | ±0.28 | ±0.009 | ±0.0093 | ±1.9 | ±1.6 | ±0.8 | | |
| 21423+0555 | HU 280 | 80.77 | 2020.46 | 0.721 | 0.1778 | 198.2 | 103.3 | 51.8 | 2 | USN2006a |
| 107153 | | ±2.52 | ±0.15 | ±0.024 | ±0.0074 | ±4.9 | ±2.9 | ±2.2 | | |
| 21477–3054 | FIN 330 AB | 20.218 | 2007.26 | 0.427 | 0.1240 | 31.9 | 215.2 | 108.4 | 2 | Doc2013d |
| 107608 | | ±0.134 | ±0.16 | ±0.026 | ±0.0016 | ±1.2 | ±3.1 | ±0.9 | | |
| 21522+0538 | JOD 23 AB | 9.08 | 2019.386 | 0.447 | 0.1406 | 163.7 | 0.0 | 0.0 | 4 | Tok2019c |
| 107948 | | ±0.11 | ±0.024 | ±0.008 | ±0.0013 | ±1.2 | fixed | fixed | | |
| 22056–5858 | B 548 | 77.03 | 2019.8 | 0.186 | 0.265 | 210.9 | 54.0 | 73.0 | 3 | SOAR2019 |
| 109060 | | ±1.45 | ±3.9 | ±0.048 | ±0.006 | ±1.7 | ±23.1 | ±1.3 | | |
| 22220–3431 | B 557 Aa,Ab | 107.97 | 2020.025 | 0.893 | 0.3559 | 190.0 | 72.8 | 112.6 | 3 | Tok2019h |
| 110419 | | ±4.79 | ±0.133 | ±0.019 | ±0.0290 | ±1.9 | ±1.7 | ±2.4 | | |
| 22342–1841 | HU 389 | 186.0 | 2006.32 | 0.417 | 0.2995 | 122.5 | 158.9 | 50.6 | 3 | Tok2019h |
| 111406 | | ±12.2 | ±1.24 | ±0.024 | ±0.0085 | ±2.6 | ±2.8 | ±1.7 | | |
| 22474+1749 | WSI 93 | 25.45 | 2017.372 | 0.634 | 0.2391 | 1.6 | 88.8 | 34.2 | 3 | Tok2017c |
| 112506 | | ±1.27 | ±0.030 | ±0.014 | ±0.0083 | ±4.6 | ±5.5 | ±1.8 | | |
| 22479–5705 | B 2059 | 43.17 | 2007.00 | 0.70 | 0.125 | 71.9 | 176.0 | 102.1 | 3 | SOAR2019 |
| 112561 | | ±2.82 | ±2.70 | fixed | ±0.007 | ±4.4 | ±24.7 | ±3.7 | | |
| 22532–3750 | HDS3250 Aa,Ab | 10.62 | 2011.77 | 0.28 | 0.1395 | 226.0 | 100.1 | 56.7 | 4 | SOAR2019 |
| 113010 | | ±1.51 | ±0.17 | ±0.13 | ±0.0053 | ±4.7 | ±12.4 | ±5.8 | | |
| 23036–4651 | WSI 139 | 14.50 | 2015.48 | 0.230 | 0.2572 | 153.3 | 162.4 | 93.8 | 3 | SOAR2019 |
| ... | | ±2.15 | ±0.44 | ±0.059 | ±0.0257 | ±0.8 | ±14.7 | ±0.5 | | |
| 23210+1715 | WSI 11 | 7.95 | 2020.44 | 0.372 | 0.0852 | 163.7 | 22.9 | 28.7 | 3 | Tok2017c |
| 115288 | | ±0.10 | ±0.18 | ±0.043 | ±0.0042 | ±16.8 | ±18.1 | ±10.1 | | |

^a References to VB6 are provided at
<http://ad.usno.navy.mil/wds/orb6/wdsref.txt>

Table 6
Preliminary visual orbits

| WDS | Discov. | P (yr) | T (yr) | e | a (arcsec) | Ω (deg) | ω (deg) | i (deg) | Grade | Ref. ^a |
|------------|---------------|-------------|-------------|-------|-----------------|-------------------|-------------------|--------------|-------|-------------------|
| 00325–6800 | DON 7 | 150 | 2037.8 | 0.186 | 0.608 | 175.0 | 337.0 | 180.0 | 4 | SOAR2019 |
| 00345–0433 | D 2 AB | 777 | 2008.5 | 0.79 | 1.111 | 83.1 | 270.4 | 77.6 | 4 | Hrt2010a |
| 02128–0224 | TOK 39 Aa,Ab | 0.2595 | 1989.5599 | 0.689 | 0.0144 | 241.0 | 74.3 | 30.0 | 3 | SOAR2019* |
| 03178–1407 | HU 432 | 73.67 | 1979.23 | 0.152 | 0.2017 | 45.4 | 223.2 | 40.4 | 4 | SOAR2019 |
| 05190–2159 | RST2375 | 164.019 | 2015.515 | 0.326 | 0.3205 | 154.4 | 262.0 | 51.8 | 4 | Hrt2011d |
| 05505–5246 | B 1493 | 113.0 | 2005.00 | 0.67 | 0.1625 | 247.9 | 170.2 | 140.5 | 4 | SOAR2019 |
| 06515+0358 | A 1956 | 110.9 | 2002.6 | 0.437 | 0.3705 | 67.2 | 354.5 | 115.1 | 4 | SOAR2019 |
| 08342–0957 | HDS1226 | 54.6 | 2003.13 | 0.386 | 0.203 | 202.6 | 113.6 | 119.5 | 4 | SOAR2019 |
| 08582+1945 | LDS3836 | 134.4 | 2006.25 | 0.661 | 3.234 | 38.5 | 91.0 | 20.0 | 5 | SOAR2019 |
| 09074–4357 | B 1646 AB | 208 | 2029.4 | 0.60 | 0.188 | 15.9 | 161.1 | 116.2 | 4 | SOAR2019 |
| 09077+1040 | CHR 257 | 80.9 | 2030.06 | 0.55 | 0.201 | 106.2 | 170.7 | 79.2 | 3 | SOAR2019 |
| 09370–2610 | WSI 127 | 31.98 | 2010.47 | 0.0 | 0.3907 | 284.0 | 0.0 | 0.0 | 5 | SOAR2019 |
| 09393–1013 | RST3652 | 500 | 2002.254 | 0.70 | 1.355 | 277.7 | 96.1 | 113.7 | 5 | SOAR2019 |
| 10038–0823 | HDS1454 | 32.74 | 2010.60 | 0.70 | 0.087 | 177.9 | 334.6 | 124.8 | 4 | SOAR2019 |
| 10193–1232 | RST3688 | 180 | 2005.08 | 0.544 | 0.6852 | 142.1 | 278.5 | 80.9 | 4 | SOAR2019 |
| 10476–1538 | TOK 714 Aa,Ab | 9.32 | 2015.59 | 0.103 | 0.0572 | 120.2 | 43.3 | 117.1 | 4 | SOAR2019 |
| 11064–3545 | DAW 132 AB | 163.3 | 1983.62 | 0.97 | 1.199 | 121.8 | 177.4 | 141.2 | 5 | SOAR2019 |
| 11342+1101 | YSC 43 Aa,Ab | 10.97 | 2005.44 | 0.522 | 0.0666 | 351.8 | 77.2 | 101.3 | 4 | SOAR2019 |
| 11495–1636 | TOK 717 Aa,Ab | 24.0 | 2018.05 | 0.145 | 0.1984 | 292.5 | 108.2 | 102.6 | 4 | SOAR2019 |
| 13327+2230 | HDS1898 | 30.0 | 2001.8 | 0.82 | 0.3056 | 251.0 | 94.1 | 74.0 | 3 | FMR2013d |
| 13344–4224 | SEE 182 | 480 | 2017.290 | 0.983 | 1.073 | 28.1 | 288.0 | 55.0 | 5 | SOAR2019 |
| 13344–5931 | TOK 403 | 18.44 | 2021.11 | 0.385 | 0.1441 | 77.2 | 265.5 | 117.7 | 4 | SOAR2019 |
| 14038–6022 | VOU 31 AB | 182.0 | 2031.30 | 0.60 | 0.788 | 251.9 | 171.8 | 125.4 | 4 | SOAR2019 |
| 15234–5919 | HJ 4757 | 600 | 2111.7 | 0.404 | 1.275 | 123.9 | 218.7 | 127.8 | 4 | Hrt2010a |
| 16038+1406 | HDS2265 | 53.7 | 2021.17 | 0.815 | 0.3544 | 1.3 | 153.1 | 63.6 | 4 | Tok2018e |
| 17012–1213 | HU 163 | 160 | 2009.0 | 0.73 | 0.1994 | 154.7 | 28.6 | 93.8 | 4 | SOAR2019 |
| 19197–2836 | B 433 AB | 250 | 2027.51 | 0.458 | 0.441 | 219.7 | 97.7 | 57.2 | 4 | SOAR2019 |
| 19563–3137 | TOK 698 | 13.0 | 2016.29 | 0.292 | 0.1063 | 59.8 | 44.0 | 90.8 | 4 | SOAR2019 |
| 20521+0205 | A 2286 AB | 273.0 | 2015.07 | 0.687 | 0.311 | 83.3 | 226.8 | 60.6 | 4 | SOAR2019 |
| 21477–1813 | CHR 223 | 73.829 | 2025.728 | 0.311 | 0.1713 | 110.9 | 275.3 | 109.9 | 4 | Tok2015c |
| 21491–7206 | HEI 598 | 120 | 2016.44 | 0.349 | 1.565 | 42.8 | 67.8 | 51.8 | 4 | SOAR2019 |

Table 6 — *Continued*

| WDS | Discov. | P (yr) | T (yr) | e | a (arcsec) | Ω (deg) | ω (deg) | i (deg) | Grade | Ref. ^a |
|------------|------------|-------------|-------------|-------|-----------------|-------------------|-------------------|--------------|-------|-------------------|
| 22266–1645 | SHJ 345 AB | 3500 | 2020.45 | 0.913 | 14.558 | 289.1 | 158.4 | 34.3 | 4 | Hle1994 |
| 22378–5004 | HDS3214 | 82.7 | 2020.14 | 0.75 | 0.145 | 110.6 | 64.3 | 138.0 | 4 | Tok2019d |
| 22441+0644 | TOK 703 | 5.02 | 2015.93 | 0.316 | 0.0585 | 168.7 | 166.5 | 134.3 | 4 | SOAR2019 |

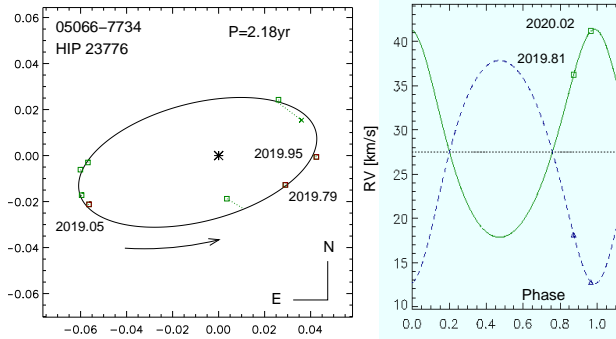


Figure 5. Combined preliminary spectro-interferometric orbit of HIP 23776.

^a References to VB6 are provided at <http://ad.usno.navy.mil/wds/orb6/wdsref.txt>

4. SUMMARY

Continued monitoring of close visual binaries at SOAR results in gradual improvement of the orbits, especially for tight and nearby pairs with short periods like HIP 23776 (Figure 5). Good-quality visual orbits coupled to precise parallaxes from *Gaia* will vastly extend our knowledge of stellar masses. Knowledge of visual orbits is needed in various astrophysical contexts, for example for binaries hosting exoplanets.

The SOAR speckle program has resulted in the discovery of many new close binaries and subsystems. This list is extended here by the 90 new pairs, although *Gaia* reveals some wide and faint new companions as unrelated (optical). During 2019, the core program on visual multiples has been supplemented by various binary surveys like high-resolution follow-up of TESS exo-planet candidates and the multiplicity survey of Upper Scorpius association.

We thank the SOAR operators for efficient support of this program, and the SOAR director J. Elias for allocating some technical time. This work is based in part on observations carried out under CNTAC programs CN2019A-2 and CN2019B-13.

R.A.M. and E.C. acknowledge support from the Chilean Centro de Excelencia en Astrofísica y Tecnologías Afines (CATA) BASAL AFB-170002, and FONDECYT/CONICYT grant # 1190038.

This work used the SIMBAD service operated by Centre des Données Stellaires (Strasbourg, France), bibliographic references from the Astrophysics Data System maintained by SAO/NASA, and the Washington Double Star Catalog maintained at USNO. This work has made use of data from

the European Space Agency (ESA) mission *Gaia* (<https://www.cosmos.esa.int/gaia>) processed by the *Gaia* Data Processing and Analysis Consortium (DPAC, <https://www.cosmos.esa.int/web/gaia/dpac/consortium>). Funding for the DPAC has been provided by national institutions, in particular the institutions participating in the *Gaia* Multilateral Agreement.

Facilities: SOAR.

REFERENCES

- Benedict, G. F., Henry, T. J., Franz, O. G., et al. 2016, *AJ*, 152, 141
- Calissendorff, P., Janson, M., Köhler, R., et al. 2017, *A&A*, 604, 82
- Gaia* Collaboration, Brown, A. G. A., Vallenari, A., Prusti, T., et al. 2018, *A&A*, 595, 2 (Vizier Catalog I/345/gaia2).
- Goldin, A. & Makarov, V. V. 2006, *ApJS*, 166, 341
- Hartkopf, W. I., Mason, B. D. & Worley, C. E. 2001, *AJ*, 122, 3472
- Hartkopf, W. I., Tokovinin, A. & Mason, B. D. 2012, *AJ*, 143, 42
- Horch, E. P., van Belle, G. T., Davidson, J. W., Jr. et al. 2015, *AJ*, 150, 151
- Horch, E. P., Casetti-Dinescu, D. I., Camarata, M. A., et al. 2017, *AJ*, 153, 212
- Horch, E. I., Tokovinin, A., Weiss, S. A., et al. 2019, *AJ*, 157, 56
- Mason, B. D., Wycoff, G. L., Hartkopf, W. I., et al. 2001, *AJ*, 122, 3466 (WDS)
- Mason, B. D., Hartkopf, W. I., Miles, K. N., et al. 2018, *AJ*, 155, 215
- Mendez, R. A., Claveria, R. M., Orchard, M. E., & Silva, J. F. 2017, *AJ*, 154, 187
- Nordström, B., Mayor, M., Andersen, J., et al. 2004, *A&A*, 419, 989
- Perryman, M. A. C., Lindegren, L., Kovalevsky, J. et al. 1997, *A&A*, 323, L49
- Tokovinin, A. 2012, *AJ*, 144, 56
- Tokovinin, A. 2016a, *AJ*, 152, 138
- Tokovinin, A. 2016b, ORBIT: IDL software for visual, spectroscopic, and combined orbits. Zenodo, doi:10.2581/zenodo.61119
- Tokovinin, A. 2018a, *PASP*, 130, 5002
- Tokovinin, A. 2018b, *ApJS*, 235, 6
- Tokovinin, A. 2019, *Inf. Circ.*, 199, 1
- Tokovinin, A. & Briceño, C. 2020, *AJ*, 159, 15
- Tokovinin, A., Cantarutti, R., Tighe, R., et al. 2010b, *PASP*, 122, 1483
- Tokovinin, A., Cantarutti, R., Tighe, R., et al. 2016b, *PASP*, 128, 125003
- Tokovinin, A., Mason, B. D., & Hartkopf, W. I. 2010a, *AJ*, 139, 743 (TMH10)
- Tokovinin, A., Mason, B. D., & Hartkopf, W. I. 2014, *AJ*, 147, 123
- Tokovinin, A., Mason, B. D., Hartkopf, W. I., et al. 2015, *AJ*, 150, 50
- Tokovinin, A., Mason, B. D., Hartkopf, W. I., et al. 2016a, *AJ*, 152, 116
- Tokovinin, A., Mason, B. D., Hartkopf, W. I., et al. 2018, *AJ*, 155, 235
- Tokovinin, A., Mason, B. D., Mendez, R. A., et al. 2019, *AJ*, 158, 148
- Ziegler, C., Tokovinin, A., Briceño, C., et al. 2020, *AJ*, 159, 19